Proton acceleration in the high contrast regime

The experimental campaign took place in the *Salle Jaune* between January 2007 and April 2008. Despite its long duration, it brought to roughly two months of laser time. The beginning of the experiment coincided with the re-opening of the laser installation after important upgrades of the system, notably the installation of the XPW stage and related devices, with the consequent rebuilt of the entire front-end. The third amplification stage (4-pass, $\times 20$) passed from cryogenic to water-chilled, which re-opened the problem of thermal lensing, needing static (refractive) correction. As a consequence the phase front worsens and day to day variation of the beam divergence is observed; moreover the refractive correction is calculated for a fixed thermal gradient in the crystal, hence for a precise flux of laser pumps. The user is not anymore free to continuously change the laser output energy.

This experimental campaign also aims to test, for the first time, the new proton diagnostic back-end, which includes the use of image plates to monitor the beam direction and divergence and the MCP-based Thomson Parabola setup (6.2.2).

In this chapter I focus on the results that are obtained with the setup described in Ch.6. The first part is dedicated to the results that are published in literature and that represent the present horizon of this topic. A second part is dedicated to the description of the experimental procedure that have been defined during the experiment. Finally the results are extensively presented and discussed.

7.1 Previous Works

The laser ion acceleration was first obtained by Gitomer et al.[36] in 1986, after the growing interest in late seventies on the presence of ion signals of different species coming from laser produced plasmas[18, 19]. Since then, a number of experiments have been performed, to understand the correlation between the characteristics of the accelerated charge (cutoff energy, relative importance of the different species, direction of emission and beam divergence) and the target (material, thickness) and laser parameters (energy, shape, peak intensity). The maximum energy with a long pulse, high energy laser[1] was obtained by Snavely et al. [93, 41] in 2000 on a $125\mu m$ thick aluminum target, with a proton energy cutoff of $E_{MAX} = 58MeV$. In the short pulse, low energy limit, the highest energy ever achieved is $E_{MAX} = 12MeV$ on the *Salle Jaune* laser system by S. Fritzler in 2003 [28] on a $10\mu m$ thick aluminum foil. Two other independent experiments, [79] for $\tau_L = 400fs$, $I_0 = 6.010^{18}W/cm^2$ and [77] for $\tau_L = 450fs$, $I_0 = 5.510^{18}W/cm^2$ report proton energies above $10MeV$ The energy spectrum is a Maxwellian-like distribution with a defined cutoff. The divergence of the proton beam changes depending to the proton energy, and the higher the energy, the lower the divergence. In [15] a divergence of $10°$ (FWHM) for $10MeV$ protons is measured.

Origin of the proton signal As discussed in 3.4, the expansion of a plasma where a difference in temperature exists between the electron and the ion population, produces the strong acceleration of the ions in the peripheral region. The origin of a proton signal among the different ion species is found in the contamination of the target's surfaces by hydrogenated compound (H_2O, organic molecules). This is in accord with the presence of a proton signal independently of the target material. The effect of the surface contamination has been confirmed by experiments where contaminants have been removed by target heating [66, 42] and laser ablation [67]: in these cases higher ion energies are observed, which confirms the electrostatic nature of the acceleration process.

Mechanisms of acceleration The protons are extracted and accelerated from the two exposed surfaces, the irradiated (*front*) [91, 103, 26, 79] and the non-irradiated (*rear*)[93, 102, 42]. The scientific community has been discussing long time about which of the two effects was producing the most effective acceleration. Some numerical studies

[1] $I_0 = 3 \times 10^{20}W/cm^2$ with $E_L = 48J$.

[83] showed that the most energetic and least divergent beam comes actually from the rear surface, while the front accelerated have bigger spread and lower cutoff energy. An extensive study on the correlation between the front surface accelerated ions and laser parameters has been performed by Habara et al. [40, 39] by using carbon targets that were deuterated only on one of the surfaces. Fuchs [29] experimentally showed that for a $30J$, $350fs$ laser interacting with a $20\mu m$ thick aluminum target, the most energetic protons are accelerated from the non-illuminated surface. Mackinnon [60] used a smaller intensity laser pulse to create a plasma with a gradient scale length of $100\mu m$ on the rear surface of a $25\mu m$ thick aluminum target. He observed that in conjunction with this plasma gradient, the proton energy cutoff was lowered from $21MeV$ to $< 5MeV$. In [49] is underlined that, being the front face accelerating mechanism independent from the target thickness, the front accelerated protons would take over in the spectrum when TNSA is made ineffective by target destruction. This argument is more deeply investigated in section 3.3.

Effect of laser parameters The laser parameters influence the acceleration mechanisms and the proton cut-off energy on a two-fold basis: *(i)* depending on the parameters themselves, like intensity and energy, and *(ii)* in conjunction with the some of the target parameters.

As a general rule, for a given intensity (power over surface), more energetic protons are produced by the most energetic pulse. Different situations need however to be analyzed specifically. For the front surface acceleration (3.4.1), the scaling law (3.26) shows a linear dependence between the cutoff energy and the normalized amplitude parameter $a \propto \sqrt{I_0} \propto \sqrt{E_L/\tau}$.

For the rear surface accelerated ions, no precise scaling law exist. Limiting ourselves to the dependence on the laser intensity, a simple rule can be obtained from the isothermal model (3.34)[2]. Neglecting for the moment the term in $\log()$., the energy is proportional to $k_B T_e$. From an extremely simplified calculation, one can write the electron temperature from

$$k_B T_e = (\gamma - 1) m_0 c^2 \tag{7.1}$$

[2]Note that the dependence to $k_B T_e$ outside the log() is the same in the adiabatic model (3.37)

for electrons having relativistic γ in the laser field (as defined in (2.13))[3]. For $a \gg 1$ it holds $\gamma \approx a$, which brings to $E_{max}^{(TNSA)} \propto k_B T_e \propto \sqrt{I}$. A more precise insight on the distinction between the dependence on the intensity and the dependence on the energy is presented in the discussion of the experimental results.

The dependence on the duration of the laser pulse is not completely clear. Some authors [61, 78, 68] reported of an ideal condition for the ion acceleration when the laser pulse is longer than $\tau_{recirc} = 2d/c$ where d is the target thickness. According to [61, 91] if the laser duration is higher than the time taken by hot electrons to cross twice the entire thickness, they experience a second heating on the -still- illuminated front surface after having been reflected in the Debye sheet on the rear one.

Effect of target thickness For front emitted protons, the thickness of the target plays only for its variable stopping power. Protons emitted by the illuminated surface of a thicker target will loose a larger amount of energy crossing the target bulk than those who were emitted from a thinner one. The correspondence between the measured energy and the initial energy is calculated through the numerical inversions of the continuous energy losses in a solid bulk (Fig.7.1).

In the TNSA acceleration, the charge separation depends on the density of hot elec-

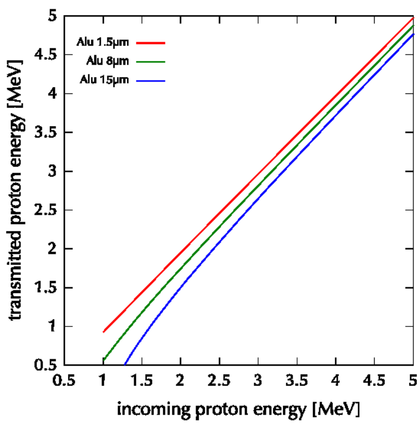

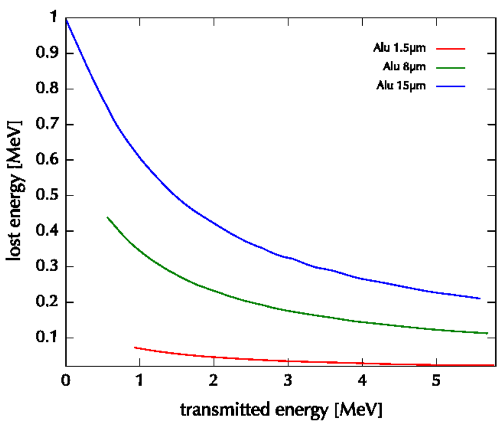

Figure 7.1: GEANT4[31, 32] simulation of proton energy loss depending on the thickness of an Aluminum bulk; *(left)* final energy vs. initial energy; *(right)* lost energy vs. final energy.

[3] $\gamma = \sqrt{a^2 + 1}$, $a = eA/mc$

trons that form the Debye sheath. The electron density n_e decreases according to the divergence in the electron transport [89, 90] through the target thickness which makes thinner targets to produce more energetic ions (Fig.7.2).

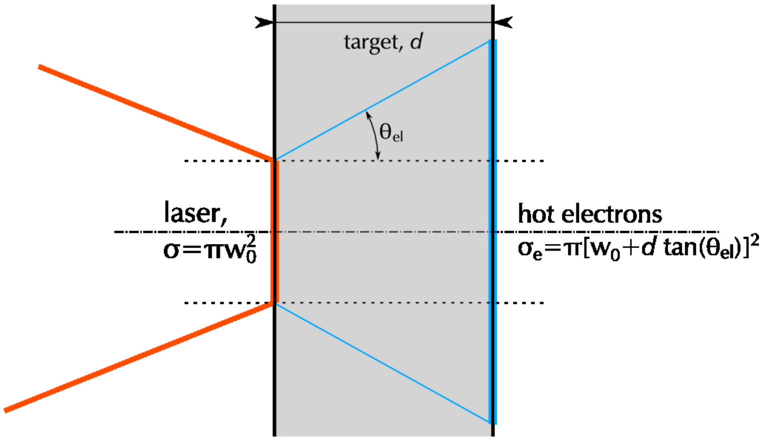

Figure 7.2: The divergence of the electron cloud being transported through the target results in a lower hot electron density on the non-irradiated surface. This adds the dependence on the target thickness for TNSA accelerated protons (neglecting the ASE and recirculation effects).

Effect of the laser pedestal In Ch.6 and Ch.3 I respectively introduced the reasons of the presence of a pedestal before the main femtosecond peak from a CPA laser chain and the effects of the heating of a metallic surface by an over-threshold intensity pulse. The production of a plasma gradient on the illuminated surface acts on the interaction mechanisms between the incoming laser peak and the electrons in the plasma: as discussed in section 3.3 the relative importance between the different interaction phenomena depends on the gradient scale length. Some authors [87] report a variation in the direction of acceleration of hot electrons as the gradient increases in length, making laser directed ponderomotive effects more important than Brunel and resonant absorption. The scale length depends on the pre-pulse intensity and on its duration. The presence of a pre-formed plasma density gradient can be beneficial for laser energy absorption and coupling to the electron component. In [4] is suggested that an optimum exists of a plasma gradient length of $L_{grad} = 4\lambda_{laser}$ in front of the target to maximize the laser absorption.

The ASE pedestal is also recognised as the main limitation to the use of thinner targets. In [49] an extensive study is presented to correlate the proton cutoff energy to the target thickness for three different pre-pulse durations. The laser peak with an intensity of $I_0 = 10^{19} W/cm^2$ is preceded by a pedestal of $\tau_{ASE} = 2.5ns$ at a contrast of 10^7. An optimum target thickness exists, and it is found to be dependent on the ASE duration. A reduction of τ_{ASE} of the 80% (from $2.5ns$ to $0.5ns$) reduces by the same factor the ideal thickness and increases the proton cutoff energy from $2.5MeV$ to $3.5MeV$. The linear variation of the ideal thickness with the ASE duration confirms the presence of a perturbation that is initiated by the ASE front itself and that travels at a finite velocity through the bulk. According to the same paper, the ideal thickness does not change when varying the laser intensity (keeping constant the contrast ratio). Nevertheless it has to be underlined that I_0 is reduced only by a factor of 0.67.
Following the argument in [49], thinner targets experience a limitation in the TNSA mechanism due to the formation of a plasma density gradient on the non-illuminated surface, as a consequence of the ASE-created shock breakout. The linear propagation law presented in [49] states

$$d_{ideal}[\mu m] \; = \; 3.6 \cdot \tau_{ASE}[ns] \tag{7.2}$$

which defines the timescale of the pre-pulse effect on the TNSA acceleration[4].

In [57] a deviation from the target normal is observed for the accelerated proton beam; it is suggested to be caused by the induced deformation and tilting of the normal direction of the rear surface, as a consequence of the shock wave breakout.

7.2 Experimental procedure

The thin aluminum foils are positioned between two nickel holders on a 5-axis (3 spatial, 2 tilts) mount. The initial focus position is set in a range of $\sim 200\mu m$ by simply looking at the speckle field that is produced by the helium-neon laser (collinear to the pump beam path) on the metallic target. This position is set as reference on the high-magnification focus reference (Fig.6.6-6). The two tilt axis are regulated so that moving

[4]This law apparently contrasts with the experimental results that are presented in Ch.5 for the reflectometry experiment. This discrepancy is discussed in 7.4.1.

the target holder in a range of 3×3 shot positions[5] doesn't change the relative focus reference by more than $50\mu m$[6]. This ensures a maximum tilt of $\sim 0.9°$ with respect to the pinhole-TP-MCP axis. The chamber is pumped down to a vacuum better than 10^{-3} and MCP is activated.

Error Estimation

The principle source of uncertainty in the experimental procedure is represented by the laser system itself. I believe that the fluctuation of its parameters can absorb all other errors on motors and image analysis. For this reason, in the rest of the chapter, the experimental the experimental proton energies are an average of many (at least three) shots of the same experimental configuration; the associated error bars are calculated from the width of distribution of the acquired data.

[5] There are $1.5mm$ between two adjacent shot positions.

[6] The perpendicularity between horizontal/vertical target movements and the MCP axis –referenced by a second Helium-Neon laser– has been previously checked by substituting the target holder with a mirror.

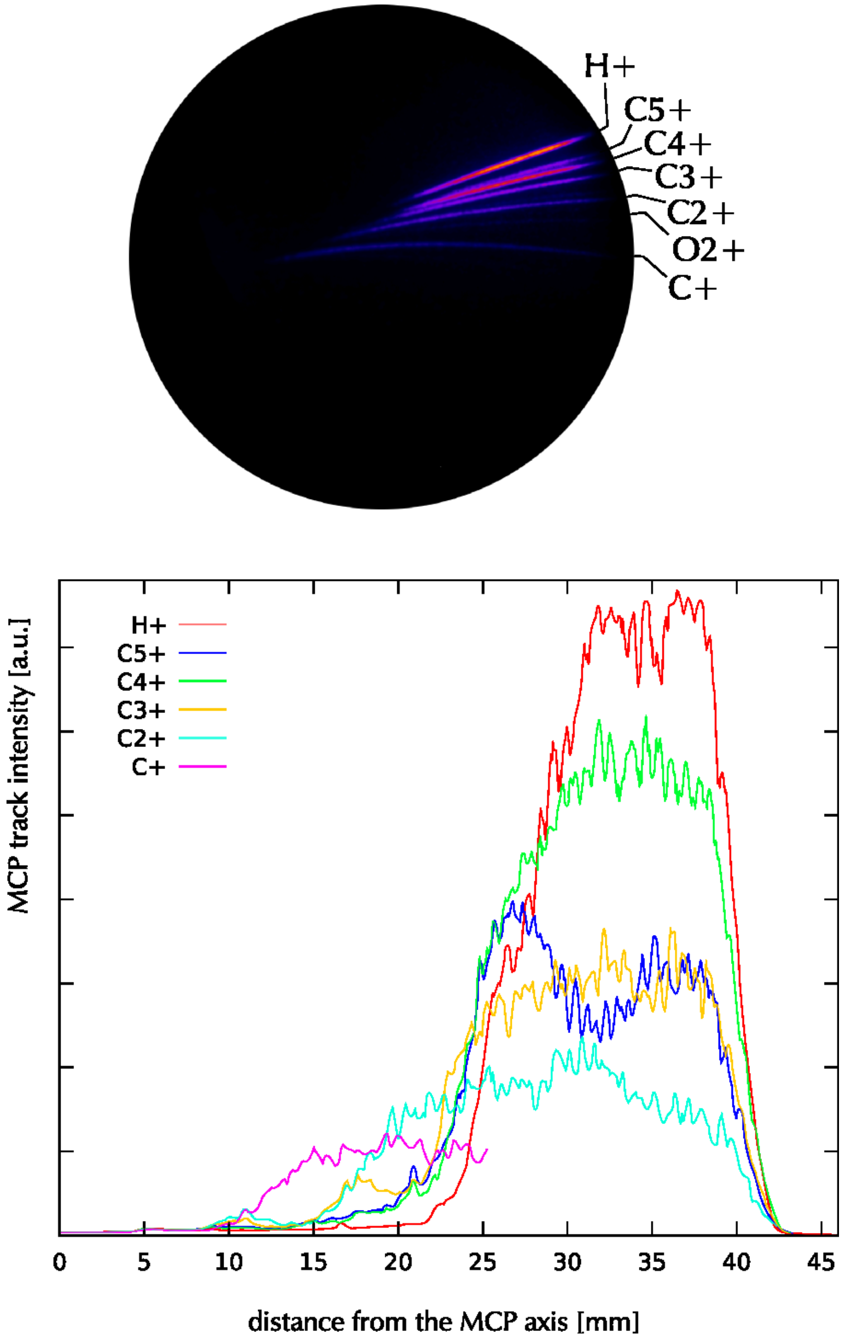

Figure 7.3: Real time result from a laser shot; *(upper)* MCP image (in fake colors) from a $d = 400nm$ aluminum target; *(lower)* spectral plot from the track on the image, obtained from spatial integration of the tracks (see Ch.6.2.2 for details on the analysis algorithm).

7.3 Validation of experimental parameters

7.3.1 Target focusing

The correct position in focus is searched from the direct experimental feedback of the proton signal: targets are moved around the first reference by steps of $25\mu m$ (which is above the resolution limit of the focus reference and about the Rayleigh depth of the parabola) and shot at least twice. According to (2.8) the peak intensity is changed which affects the expected ion energy cutoff. In the normal case, a single peak is found, well reproducing the change in intensity (Fig.7.4). The focus position is normally found no further than $150\mu m$ away from the helium-neon alignment and normal laser conditions give fluctuations lower than 10% in proton energy. In the waist, our laser and optics parameters produce a peak intensity in the order of $\sim 5 \times 10^{19} W/cm^2$.

The procedure shows two kinds of deviations from the standard behaviour: *(i)* a two-peaks structured plot and *(ii)* a flat region well wider than the expected Rayleigh range. This simple fact underlines the extreme improvement that a real time diagnostic system represents for the laser ion acceleration experiments. The two effects are now briefly discussed.

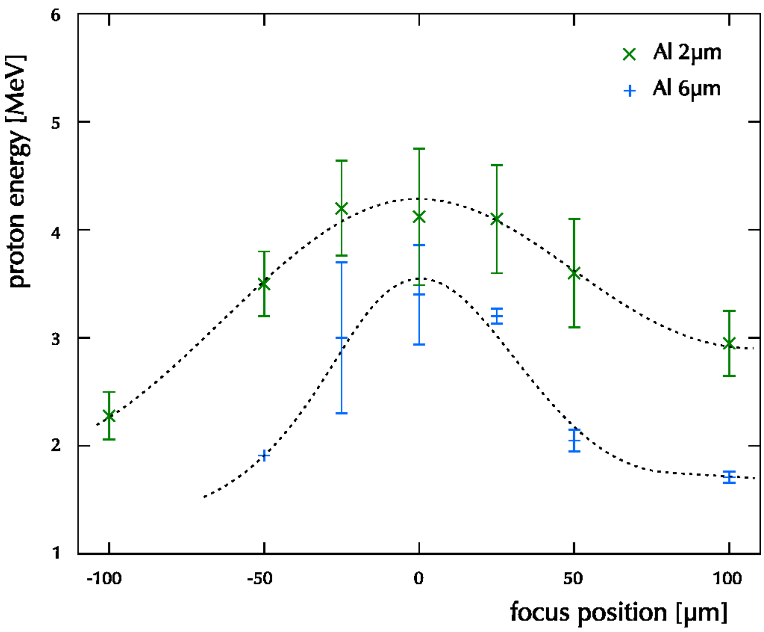

Figure 7.4: Proton cutoff energy for different focus position on Aluminum targets of 6μm and 2μm. In the entire scanned area, more energetic protons are generated from the thinner target (dashed lines are added to help visualization).

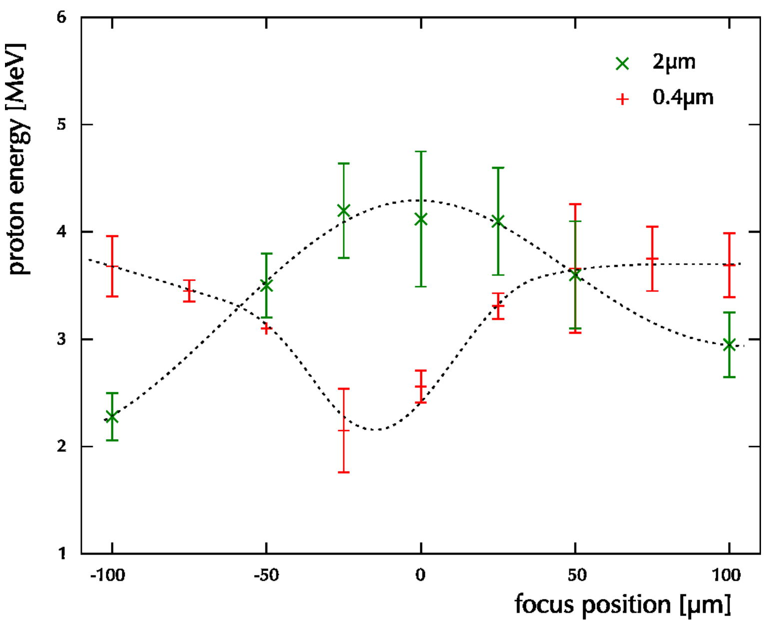

Figure 7.5: Proton cutoff energy for different focus position on Aluminum targets of 2μm and 400nm. The plot for the thinner target exhibits a minimum in the focus position where a thicker target has a maximum (dashed lines are added to help visualization).

Contrast As the target is moved away from the beam waist, the peak intensity and the pedestal intensity decrease accordingly. In the case where the used target is too thin to hold the pedestal flux in the beam waist, a reduction of the peak intensity through the movement in focus (Fig.7.6) can produce better interaction conditions. In this case two peaks appears in the focus scan, symmetric around the beam waist (Fig.7.5). When this situation happens, even measurements from thicker targets have to be discarded.

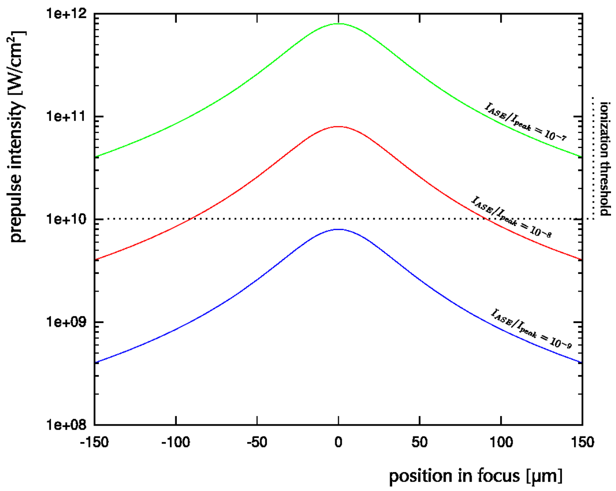

Figure 7.6: Theoretical pedestal flux for a 2.5ns pre-pulse at different contrast ratios.

Beam Aberrations It's been reported in literature of experiments where the proton energy cutoff seemed to be less sensitive than expected to the position of the target on the laser propagation direction. A proton signal of almost constant energy is sometimes found in a range in focus that is bigger than the supposed Rayleigh depth. The described case is showed in Fig.7.7. We believe this to be caused by a highly deformed phase front, possibly in conjunction with a misalignment of the parabola (which introduces strong astigmatism). In these cases the intensity distribution is not gaussian anymore and the peak intensity is less sensitive to the focus position. Moreover the quality of the beam in its waist is worsened, which produces less energetic ions even at the best focus position. This effect is normally removed by acting on the parameters of the deformable mirror (specially the radius of curvature) or the alignment of the parabola.

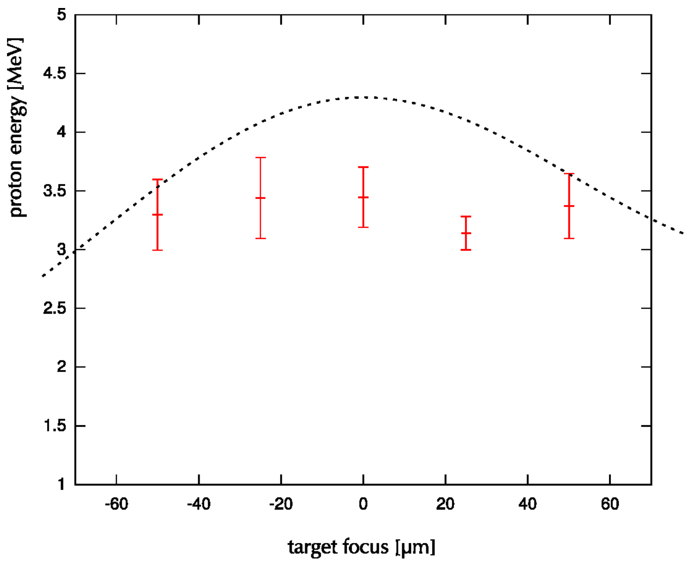

Figure 7.7: Maximum proton energy for different positions of a $6\mu m$ thick Aluminum foil. The dashed line is the same as Fig.7.4.

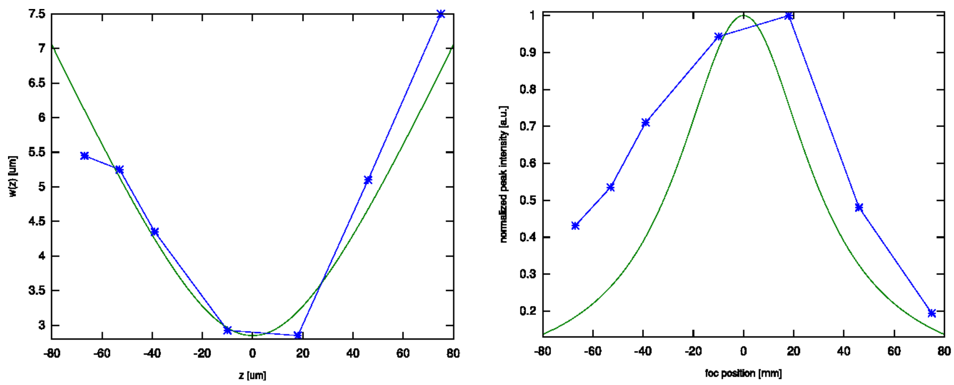

Figure 7.8: Comparison between the laser transverse profile at different positions around the focal spot (from images recorded by the camera) and a perfect gaussian beam; (*left*) waist size, (*center*) normalized peak intensity. The theoretical Rayleigh range is $z_0 = 34\mu m$.

.

7.3.2 MCP Calibration and Alignment

The MCP-based diagnostic system has to be validated from the point of view of *(i)* the direction of the measure, i.e. the solid angle where the incoming charge is collected, and *(ii)* the absolute measure of the proton energy.

In the realized setup, the MCP entrance pinhole sets a solid angle of beam integration of $\sim 5 \times 10^{-8}$sr that corresponds to an horizontal sweep angle of ~ 0.25mrad. This axis is fixed on the chamber axis. As previously discussed in section 7.2, the targets are aligned to a tilt better than $\sim 0.9°$ to the chamber axis. The typical half divergence of the more energetic part of the ion beam is in the order of $7°$ to $10°$ [15] which makes our alignment good enough not to miss the main beam. Nevertheless the possibility of a misalignment of the ion beam due to pre-pulse effect have to be considered, to ensure the self-consistency of the acquired data. In [56, 88, 57], the deformation of the rear target surface induced by the emerging shock wave is considered responsible of a lateral drift of the most energetic part of the ion beam, towards the laser axis. Given $\Delta\theta_P$ the half divergence of the highest energy part of the beam and θ_P the described deviation on the horizontal plane, in the typical case of $\theta_P = 5°$ and $\Delta\theta_P = 10°$ [7], the remaining uncertainty due to target tilt must be lower than $\sim 5°$. As a general precaution, whenever contrast effect like the one in Fig.7.5 are observed on the thinnest target, any other data from thicker foils is discarded.

Proton energy calibration The maximum proton energy is calculated from the distance between the cutoff of the proton track and the measured zero point. The distance is converted in microns and the calibration curve for the dispersion in the magnetic field (6.2.2) interpolated to find the corresponding energy. To validate the energies that are obtained in this way (so to validate the entire process in detection, measure and calibration of the Thomson Parabola), a certain number of shots has been repeated on MCP and on multiple CR39 foils covered by filters of appropriate stopping power.

7.4 Proton Acceleration with Enhanced Contrast Laser

This section is dedicated to the results that are obtained during the experimental campaign. The proton beam is generated varying the different parameters that enters in the interaction, the thickness of targets, the laser energy and the duration of the pulse. The last two do couple together in changing the flux on the target; crossing the two scans separates the correlation between the proton cutoff energy and the intensity/energy effects. In order to underline the dependence on laser contrast, the results are compared with the experimental data that was obtained by A. Tafo[96] on the same laser chain

[7] From [57] for $4MeV$ protons from Aluminum target with $3ns$ pre-pulse at 10^7 contrast.

(before the XPW was inserted) and what is obtained by T. Ceccotti et. al [12] at the CEA-Saclay with a double plasma mirror.

Laser Conditions

If not specified otherwise, the experimental data here presented are obtained with a total laser energy of $1.5J$ before compression and a contrast better than 10^9 up to $500ps$ before the main peak.

7.4.1 Correlation with Target Thickness

The proton signal is recorded from targets of different thicknesses, from $15\mu m$ to $400nm$ at the best focus position. The evolution of the proton energy cutoff (Fig.7.9, red points) shows a meaningful dependence. In the direction of increasing thickness the proton en-

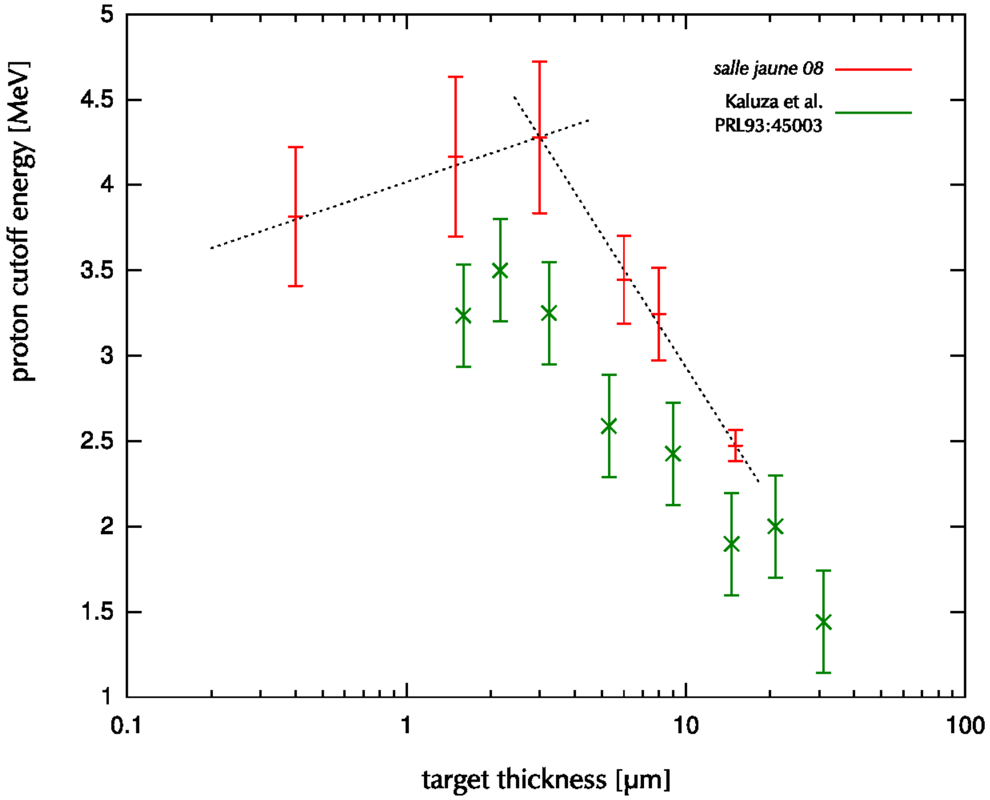

Figure 7.9: Correlation between proton cutoff energy and target thickness. The experimental data *(red)* is compared with points *(green)* from Kaluza[49] Fig.1 for $I = 1.0 \times 10^{19} W/cm^2$ and $t_{ASE} = 0.5ns$.

ergy decreases, consistently with the increased spread of the electron cloud, travelling through the thicker target. An ideal thickness is found for $d = 2\mu m$.
The *green* set in Fig.7.9 reports, for comparison, the points from the best contrast case in [49], for a contrast of 10^7 and a pre-pulse cut to $0.5ns$ from the main pulse, at $I = 10^{19} W/cm^2$([8]). Our data on the plot changes in derivative around $2\mu m$ thickness: for lower thicknesses the proton cutoff energy is found to decrease. It is important to underline that the behaviour in the two cases is qualitatively different. In our experimental case the supposed detrimental effect of the pre-pulse has a timescale which is longer than expected. Over a span of $\times 5$ in target thickness (from $400nm$ to $2\mu m$) the decrease in energy is around the 10%, and almost absorbed in the error bars. In the cited paper it is suggested that the ion signal for thicknesses $d < d_{ideal}$ could be produced mostly by front surface acceleration, achieving lower energies but remaining active even when TNSA is made ineffective by the plasma expansion on the rear surface. Since the scaling in energy for front face acceleration is only due to the stopping power of the target, this would in principle explain why in our scan (Fig.7.9) the proton cutoff energy remains almost constant; in fact (see Fig.7.1) for $E_p \sim 4MeV$ and $d < 2\mu m$, the stopping power would account for less than $100keV$ of energy loss. Nevertheless, if the $4MeV$ signal were originated from the front surface, higher energies on targets at $d > 2\mu m$ should have been observed. A possible explanation might instead come from [73]. The ion acceleration during the expansion of the high electron temperature plasma is limited by the presence of a density gradient in the cold ion distribution (see section 3.4.2). The timescale of the expansion of this gradient is bound to the electron temperature that is produced by the shock itself. The difference between the two plots in the figure can be explained by two experimental conditions with a very different contrast level (10^7 vs. 10^9) although with comparable τ_{ASE}.

Estimation of the Contrast

If we follow the argument in [49] for the presence of an ideal thickness, the plot in Fig.7.9 enables us to infer an estimation of the duration of the laser pedestal. The reflectometry measurements showed a shock wave that propagates at a speed of $15\mu m/ns$ ((5.11)), whereas in the cited paper, the experimental fit of the ideal thickness of the target versus ASE duration gives an "effective" speed of propagation of the shock of $3.6\mu m/ns$. Considering that in Fig.7.9 the optimal thickness is $1.5\mu m$, from the two speeds I get

[8]For proton energy comparison it should be taken in account that green points are for $\tau = 150fs$, $w_0 = 2.5\mu m$ and $E_L = 510mJ$.

$$100ps \ < \ \tau_{ASE,estim} \ < \ 400ps \tag{7.3}$$

7.4.2 Correlation with Laser Energy and Pulse Duration

Energy The proton spectra are recorded varying the energy in the laser pulse but keeping the optimal compression ($\tau < 35fs$). The energy is varied by inserting neutral optical densities of different thicknesses at the end of the laser chain, just before the compressor, to attenuate the intensity of factors $10^{-1/3}$, $10^{-2/3}$ and 10^{-1}. The proton energy cutoff is shown in Fig.7.10-*(upper)*. The continuous lines are $E_p \propto \sqrt{I_0}$ and $E_p \propto \log(I_0)$ to show how the scaling in intensity changes from the first to the second dependence as target gets thicker. The reason of this behaviour is not clear. A still unconfirmed hypothesis suggests that the target thickness may act on the weight of the logarithmic term in the relationship (3.34)

Pulse duration The duration of the pulse is increased by acting on the separation between the gratings in the compressor, which produces a longer and chirped pulse. The proton cutoff energies are plotted in Fig.7.10-*(lower)*; to ensure that no dependence on the chirp sign exists, the gratings are moved in the two directions (increasing and decreasing their separation, thus producing a negative and a positive chirp) and the couples of points that correspond to the same pulse duration, superposed. The behaviour for the two shown thicknesses is different. From the thinner one ($d = 1.5\mu m$), the proton cutoff energy decreases monotonically with the laser peak intensity; on the thicker one ($d = 15\mu m$) we observe *(i)* a smaller sensitivity on the pulse duration and *(ii)* the presence of an ideal duration, with a maximum in proton energy that situates around $\tau_L = 200fs$. In [61] it is observed that for a pulse of a given duration, a transition in the maximum proton cutoff energy exists when the thickness becomes smaller than $d < c \cdot \tau_L/2$, which means that the laser pulse duration is longer than the time that is needed to relativistic electrons to cross twice the target thickness. The proposed explanation is that if previously heated electrons, reflected in the Debye sheath on the rear surface, arrive to the front when the laser pulse isn't over yet, a more effective heating can take place, which results in the acceleration to higher ion energies. The recirculation time is $\tau_{recirc} \simeq 2d/c$ and the recirculation condition $\tau_L > \tau_{recirc}$. In our experimental case, the optimal duration is found at $\tau_L = 200fs$ on a $d = 15\mu m$, which doesn't correspond to the expected recirculation time of $\tau_{recirc} = 100fs$.

I hypothesize that the observed maximum happens at the equilibrium between *(i)* the enhancement of the laser light absorption, as a consequence of the longer pulse tails and the slower plasma heating, and *(ii)* the decreasing of the laser peak intensity.

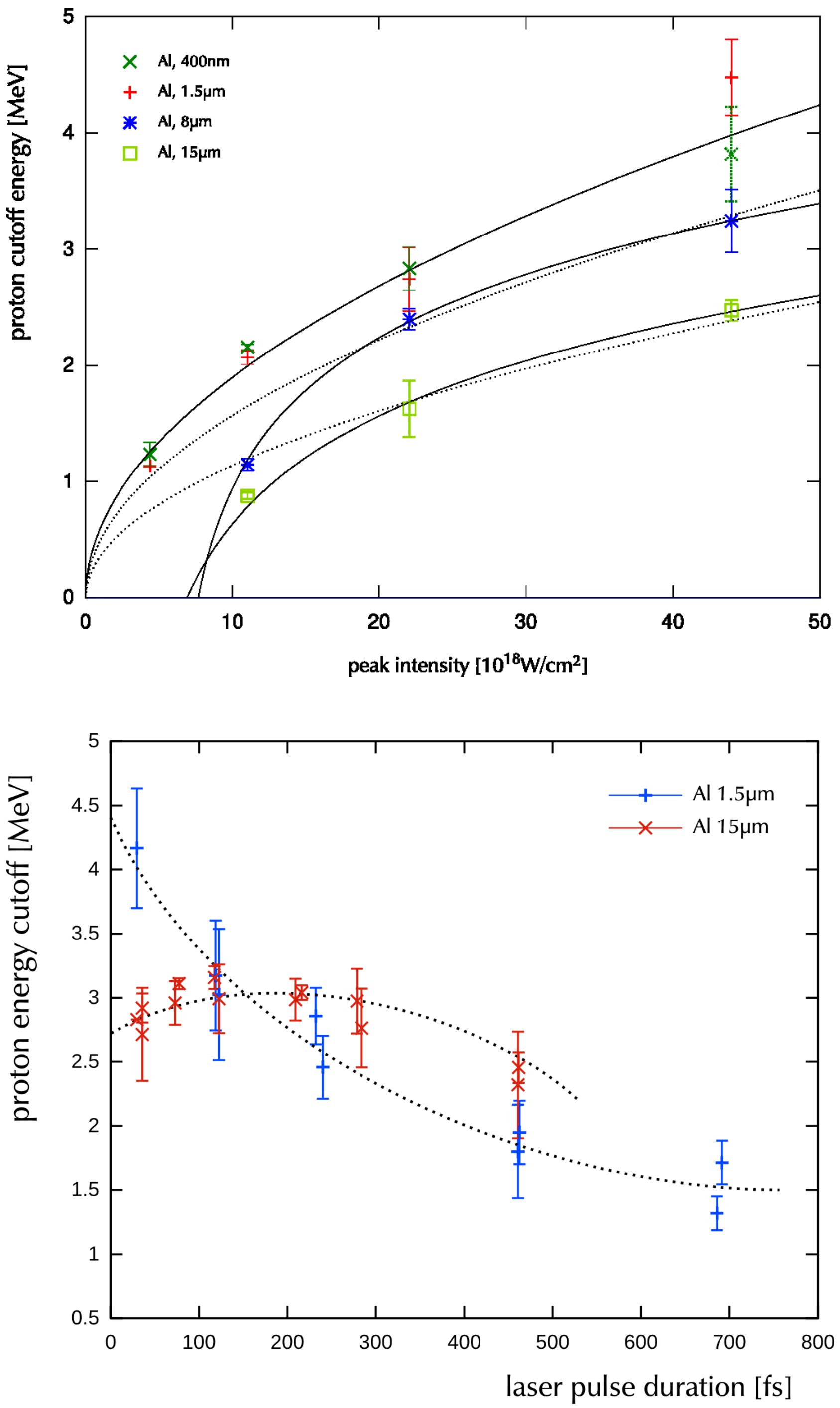

Figure 7.10: *(upper)* Scan in laser energy (laser duration is kept constant) for different target thicknesses. Black lines are plotted with $E_p \propto \sqrt{I_0}$ and $E_p \propto \log(I_0)$. Note that the point at $d = 400nm$ at the highest laser intensity has a proton energy lower than the $d = 1.5\mu m$. *(lower)* Scan in laser duration (at constant energy).

Intensity correlation In Fig.7.11 the experimental points from duration and energy scans (Fig.7.10 upper and lower) are presented in correlation of the final peak intensity for the two thicknesses $1.5\mu m$ and $15\mu m$. The qualitative difference is clear:

- The red points (duration is changed at constant energy) show a fast decrease (logarithmic) on the $d = 1.5\mu m$, and the maximum at $\tau_L = 200fs$. It is interesting to note that, for $\tau_L > 200fs$, the proton signal from the thicker target is more energetic than the one from the thinner.

- The green points (energy is changed) confirm the logarithmic behaviour for the $15\mu m$ target and a slower decrease (on the lower intensity side) for the $1.5\mu m$.

As a general rule, the emerging scenario is a more marked sensitivity on total energy for thick targets and a strong correlation to peak intensity for thinner ones.

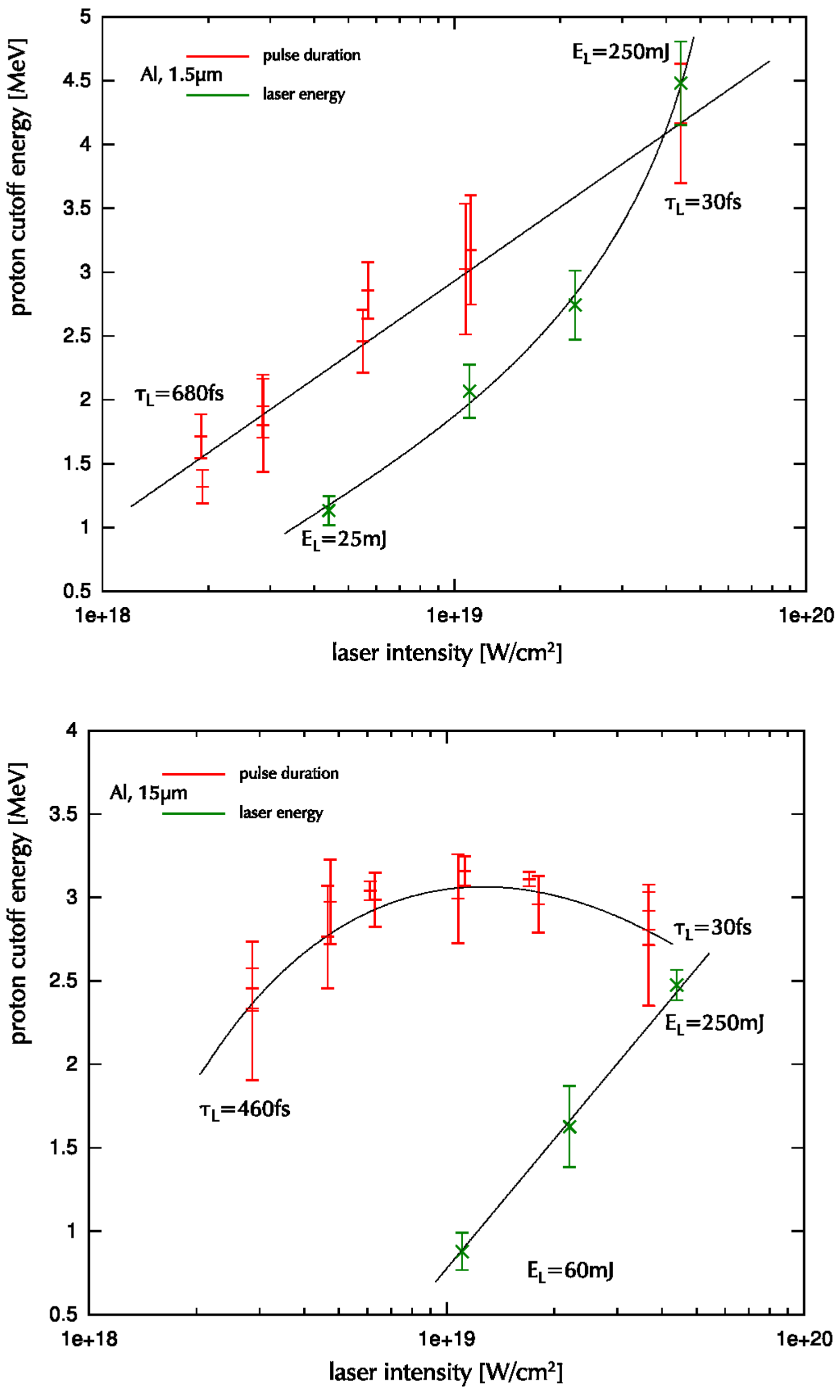

Figure 7.11: Scan in peak intensity from the experimental points in Fig.7.10 for Aluminum 1.5μm *(upper)* and 15μm *(lower)*. Red points show the behaviour for constant laser energy ($E_L = 250mJ$); green points for constant laser pulse duration ($\tau_L = 30fs$).

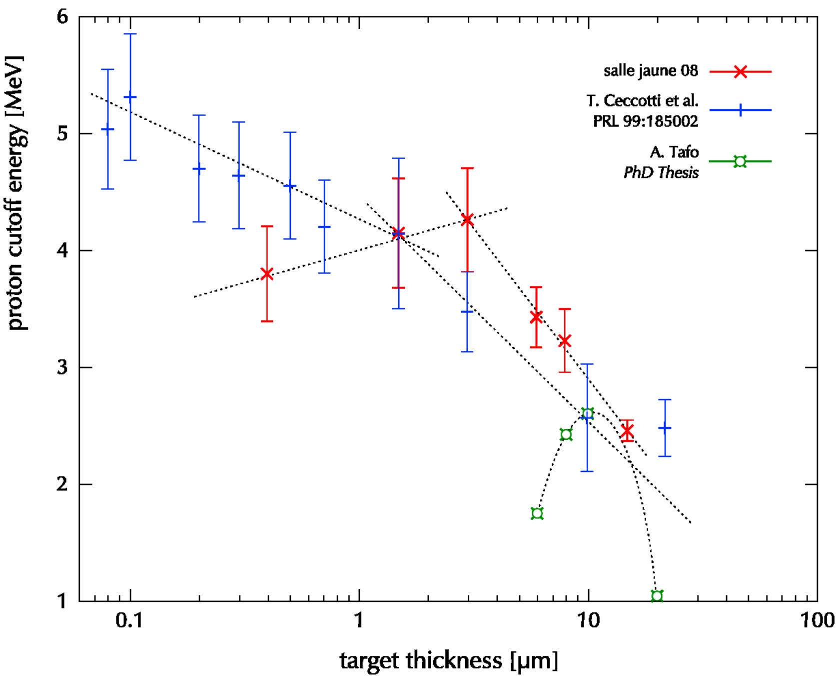

Figure 7.12: Comparison between different thickness scans. Red × are the experimental points that are reported in Fig.7.9; blue + are the results reported by T. Ceccotti et al. in [12] for $E_L = 650mJ$, $\tau_L = 65fs$ and $I_0 = 5 \times 10^{18} W/cm^2$, with a 10^{10} contrast ratio from a double plasma mirror. Green circles are the results that were obtained by A. Tafo [96] in 2004 on the *Salle Jaune* laser system before the installation of the XPW system.

7.5 Discussion and Conclusions

During the experimental campaign, ions and proton beams have been produced by the direct interaction between a laser pulse and a thin solid target. These are the first results that are produced with the XPW system for the contrast enhancement. The ion signal that is produced is stable and repeatable: in Fig.7.13 is reported the proton peak energy for 8 shots in a row, in the same experimental condition. The quality of the contrast is confirmed by the possibility to shot on thinner targets. For example in Fig.7.12 is presented the direct comparison between the proton cutoff energies with the XPW and what is obtained by T. Ceccotti et al. [12] with a double plasma mirror, which guarantee a contrast of 10^{10} and a perfectly clean pedestal. As a reference are presented, in the same image, the experimental points for a thickness scan that were obtained in 2004 by A. Tafo et al., using the *Salle Jaune* laser chain without any contrast improvement technique (the 3ω profile is presented in the upper part of Fig.6.3).

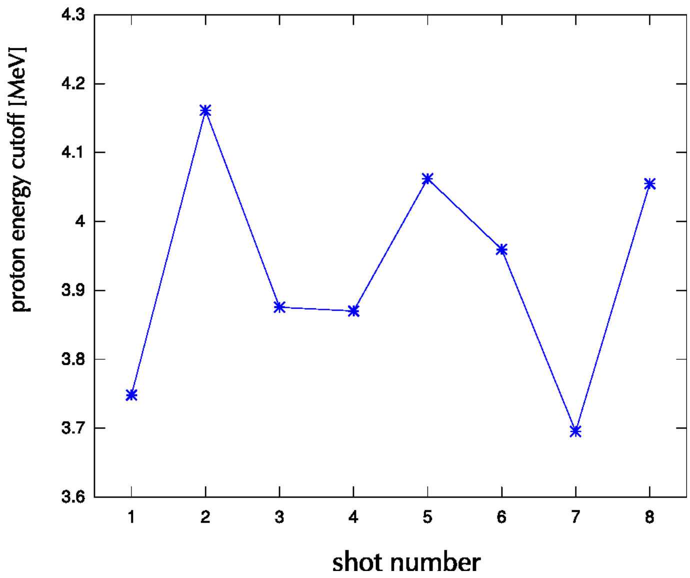

Figure 7.13: Proton cutoff energy for 8 shots in a row on $3\mu m$ thick aluminum target. The average energy is $E_p = 3.9MeV$ with a peak-to-valley fluctuation of 12%.

Further studies are needed to completely understand the experimental evidence here presented. During the very last part of the experimental campaign, a two beams experiment is set up. Here a small part of the pump beam is used to pre-heat the target surface before the interaction with the main UHI peak. The preliminary studies on front and rear face in Ch.4 and Ch.5 enable us to define the space of parameters for a pre-heating pulse, with the aim of observing the correlation between a preplasma (that is created with known parameters) and the accelerated proton beam. A preliminary analysis of the obtained results is presented in App.A.